Check for updates

Received: 29 October 2021 | Revised: 6 January 2022 | Accepted: 25 January 2022

DOI: 10.1002/er.7732

SPECIAL ISSUE RESEARCH ARTICLE

INTERNATIONAL JOURNAL OF ENERGY RESEARCH WILEY

Thermal energy storage characteristics of polyacrylic acid/dodecanol/carbon nanofiber composites as thermal conductive shape-stabilized composite phase change materials

Gökhan Hekimoğlu[1] | Ahmet Sarı[1] | Osman Gencel[2] | V.V. Tyagi[3]

[1]Department of Metallurgical and Material Engineering, Karadeniz Technical University, Trabzon, Turkey

[2]Department of Civil Engineering, Bartin University, Bartin, Turkey

[3]School of Energy Management, Shri Mata Vaishno Devi University, Katra, India

Correspondence
Gökhan Hekimoğlu and Ahmet Sarı, Department of Metallurgical and Material Engineering, Karadeniz Technical University, Trabzon 61080, Turkey.
Email: ghekimoglu@ktu.edu.tr and ahmet.sari@ktu.edu.tr

Summary

Thermal conductive shape-stabilized composite phase change materials (PCMs) were produced using polyacrylic acid (PAA), dodecanol (DDA) and carbon nanofiber (CNF) by solution blending route. In the composites, DDA was used as the material with latent heat thermal energy storage (LHTES) capability and PAA was introduced as the main supporter and shape stabilizer material for DDA. CNF was employed for two reasons: (i) to enrich the heat-storing/releasing rate of the polymer-based composite as the conductive nanofillers and (ii) to contribute to increasing the DDA adsorption rate in the shape-stabilized composites. In this regard, a series of LHTES materials were presented, comprising of PAA/DDA composite, and PAA/DDA composite PCMs doped with CNF of 4 and 10 wt%. Composite PCMs exhibited well shape stabilization performance even with a high amount of DDA (70 wt%) due to both the cross-linked spatial structure of PAA and the uniform dispersion of CNF in the composite. Fourier transform infrared spectroscopy and X-ray diffraction findings indicated that there was no chemical bonding in PAA/DDA or PAA/DDA/CNF composites. DSC analysis revealed the highly favourable LHTES properties of the PAA/DDA(70 wt%)/CNF(10 wt%) composite, melting at 18.04°C and having a phase change enthalpy as high as 157.03 J/g. The thermal gravimetric analysis results showed that this composite had excellent thermal resistance to mass degradation up to 125°C. Thermal conductivity measurements indicated the significant effect of the CNF doping on the increment of the thermal conductivity of the PAA/DDA composite. All test results suggest that especially shape-stabilized PAA/DDA/CNF composite PCM can be evaluated as energy-saving materials for thermal management of buildings.

KEYWORDS

carbon nanofiber, dodecanol, polyacrylic acid, shape-stabilized composite PCM, thermally conductivity, thermal energy storage

 © 2022 John Wiley & Sons Ltd.

1 | INTRODUCTION

The most basic requirement for all societies in the world to develop technologically and economically and have a better quality of life is energy. Today, most of the world's energy need is met from fossil fuel resources such as coal, petroleum and natural gas. However, these fossil fuel resources in the world are steadily decreasing with the increase in the energy demand caused by the reasons such as the rapidly increasing population and the continuous development of science and technology. Moreover, the excessive use of these fossil fuels has a significant effect on the increase of greenhouse gases that damage the atmosphere and cause global warming. In this case, it is becoming increasingly important to use existing energy resources more efficiently and to expand the use of alternative energy resources. Thermal energy storage (TES) technology can be evaluated as a remarkable solution in eliminating all these problems. Among different forms of advanced TES methods, implementation of phase change materials (PCMs) has become the most effective way due to their high latent heat storage density and wide temperature range for different applications.[1,2] There are various organic and inorganic substances and their mixtures researched as PCMs for thermal energy storage targets. Dodecanol (DDA) is a kind of organic-based fatty alcohol and it offers some outstanding characteristics including high LHTES capacity, good thermal reliability and cycling stability, nontoxic behaviour and low vapour pressure for low-temperature TES applications.[3,4] However, two disadvantages limit the use of organic PCMs in practical TES applications: (i) leakage problem of PCMs in the liquid phase and (ii) low thermal conductivity of PCMs causing low heat transfer rate in TES applications.[5,6,7] A well-known route to obstruct the leakage of PCMs during their phase transition is their integration with supporter materials to produce shape-stabilized PCMs, which are able to keep their solid shape above the melting temperature of PCMs.[8,9,10] Polymers and porous inorganic materials are among the most commonly used supporter materials for the shape stabilization of PCMs. Some porous inorganic matrices employed as supporter materials are expanded perlite,[11] diatomite,[12] fly ash,[13] attapulgite,[14] expanded vermiculite,[15] activated carbon,[16] silica[17] and bentonite.[18] From the other side, some typical polymer-based supporter materials studied are polyurethane,[19] polypyrrole,[20] high-density polyethylene (HDPE),[21] polyvinyl butyral,[22] polymethyl methacrylate (PMMA)[23] and polyethylene.[24] These polymer materials have a good shape stabilization function for PCMs and ensure significant merits such as high latent heat storage capacity, high thermal and chemical stability and possessing a hard and rigid morphology at atmospheric temperature. In this regard, Fauster and Feutchter[24] prepared different shape-stabilized composite PCMs comprising paraffin waxes (with different molecular weights) as PCMs and polyolefin matrix materials (polypropylene, polyethylene and ethylene/propylene copolymer) as supporter materials. Huang et al[4] studied the HDPE/cetyl alcohol shape-stabilized composite PCMs. In another study, LDPE, HDPE and LLDPE as supporter materials were employed for shape stabilization of paraffin.[25] Kee et al[26] fabricated PMMA/myristic acid shape-stabilized composite PCMs. Chen et al[27] used cellulose acetate as supporter material and polyethylene glycol (PEG) as PCM to synthesize shape-stabilized composite PCMs. Polyacrylic acid (PAA) is a type of polymer presenting high water absorbance, high chemical corrosion resistance, excellent biocompatibility, firm intermolecular interaction and high rigidity properties. Moreover, the miscibility properties of PAA make it a suitable candidate to be used as supporter materials in the production of composite PCMs.[28]

Even though such polymer-based composite PCMs can offer high shape stabilization and LHTES properties, the low thermal conductivity issue, which has been addressed above as the second main defect of PCMs, is also true of polymer-based composite PCMs. Therefore, several efficient methods have been employed to boost the thermal conductivity of polymer-based composite PCMs. An influential attempt to this deficiency is the incorporation of high thermal conductivity filler materials such as CNT, expanded graphite, graphene nanoplate (GNP), carbon nanofiber (CNF), copper particles and silver nanowires into the composite PCMs. Tian et al[29] used carbon fiber and expanded graphite as high thermal conductivity filler materials to enhance the thermal conductivity of shape-stabilized ethylene-vinyl acetate/paraffin composite. Silakhoi et al[20] combined palmitic acid, polypyrrole and GNP to synthesize shape-stabilized composite PCMs with improved thermal conductivity. He et al[2] produced shape-stabilized composite PCMs comprising of unsaturated polyester resin/PEG/GNPs. Zeng et al[30] utilized exfoliated graphite nanoplatelets to fabricate palmitic acid/polyaniline shape-stabilized PCMs with enhanced thermal conductivity. Lin et al[22] developed a series of composite PCMs containing polyvinyl butyral, palmitic acid and expanded graphite.

In this study, we aimed to fabricate shape-stabilized PAA/DDA/CNF composites as promising TES materials to be used in low-temperature thermal management applications. This study differs from other similar studies in the literature with a few different original contents: (i) even though PAA is employed in several fields, it has been very rarely utilized as supporter material for PCMs.

1099114x, 2022, 14, Downloaded from https://onlinelibrary.wiley.com/doi/10.1002/er.7732 by Bartin University, Wiley Online Library on [14/04/2023]. See the Terms and Conditions (https://onlinelibrary.wiley.com/terms-and-conditions) on Wiley Online Library for rules of use; OA articles are governed by the applicable Creative Commons License

In our extensive literature search, we have come across only one paper, published by Alkan et al,[31] in which PAA was employed as supporter material for PEG used as PCM. Apart from that study, in a few studies, PAA was used to coat polymer-based composite PCMs to prevent leakage of PCMs, rather than directly used as supporting material in the production of composite PCMs. In one of those studies, PAA was used as the sole coating material for the PMMA/myristic acid composite,[26] while in the other study, PAA and nitrile butadiene rubber mix was used as the coating material for the PMMA/myristic acid composite.[32] Lastly, PAA was utilized to produce comb-like PAA-grafted fatty alcohol polymers as TES materials through a different production approach.[33] As seen in these studies, although it is not a very distant approach to use PAA for different purposes in the production of TES materials, there is a serious lack of research and knowledge gap in evaluating it directly and solely as supporting material in the shape stabilization of PCMs. This deficiency can be considered as the first leg of the originality of this study. (ii) Again, in our comprehensive literature review, we have not found a shape-stabilized composite PCM produced via a simple solution blending method and comprising of DDA and a polymer-based supporter material. In this context, this study is also important in terms of demonstrating the potential of DDA to maintain its superior properties as a PCM also in polymer-based composites and its high compatibility with the polymer material (PAA). (iii) Herein, it is not only intended to produce a PAA-based shape-stabilized composite PCM but also to synthesize it with improved thermal conductivity for the first time in this study. Through this aim, CNF was selected to improve the thermal conductivity of the PAA/DDA shape-stabilized composite. Additionally, a specific focus is to assess the benefit of CNF nanofillers in terms of the improvement of the DDA adsorption rate in the PAA/DDA composite. In this respect, the influence of CNF on the different properties of PAA/DDA composite including adsorption capacity, LHTES features, thermal conductivity, microstructure, thermal stability and chemical structure were extensively studied. The experiment results indicated that the prepared shape-stabilized PAA/DDA/CNF composites possess favourable properties to be widely used in low-temperature LHTES applications.

2 | EXPERIMENTAL

2.1 | Materials

The PAA (Mw ~ 450 000), DDA (purity ≥98.0%) and CNF (purity >96%, outside diameter: 190 to 590 nm, specific surface area: 39 m^2/g and average pore volume: 0.12 cm^3/g) were obtained from Sigma Aldrich, while chloroform (purity ≥99) used as solvent was procured from Merck Millipore Company.

2.2 | Preparation of PAA/DDA and PAA/DDA/CNF composites

A series of composite PCMs with different ratios of PAA/DDA/CNF were synthesized. For the production of PAA/DDA composite, firstly PAA was dissolved in chloroform by mixing with a stir rod at 70°C. Following that, melted DDA was added to the solution of PAA, and the obtained mixture was stirred for 60 min at 70°C. As a final step, the mixtures were kept at 80°C for 48 h to evaporate the chloroform. On the other hand, PAA/DDA/CNF composites were produced in a similar way to PAA/DDA composites. The only difference is that the CNF was added to PAA/DDA mixture prior to the chloroform volatilization process and an additional ultrasonic mixing process was applied for 30 min for homogeneous dispersion of CNF in the solution. The preparation steps for the PAA/DDA and PAA/DDA/CNF composites were demonstrated in Figure 1.

Through the all prepared shape-stabilized composite PCMs it was aimed to find an optimum mixture ratio with the highest DDA content and also the highest heat transfer rate. To estimate these ratios, shape stabilization tests were done. During the test process, each composite sample was heated onto filter papers over at 35°C PCM for 1 h. The photographs of the produced composite PCMs with/and without CNF additive after shape stabilization test were shown in Figure 2. The composite samples with the highest PCM ratio that did not leach out after heating were determined as leak-proof composite PCMs. As can be clearly from this photograph image, for the PAA/DDA composite, the highest DDA content within the leak-proof composite was found as 33 wt%. The resistance preventing the leakage of DDA from the composite structure during heating is not only due to the weak capillary forces between the PAA-DDA but also the hydrogen bridge bond interactions formed between the C=O groups in the PAA structure and the OH groups in the DDA structure. Furthermore, the addition of CNF nanofiller to the PAA/DDA composite has been found to be beneficial in producing composites with higher DDA content. In other words, the CNF doping allowed more DDAs to be held in the hybrid matrices. That is, DDA mass percentage could be increased up to 48% in the PAA/DDA/CNF (4 wt%) shape-stabilized composite. When the CNF amount was increased to 10 wt%, the DDA mass ratio reached up to 70% within the composite without any leakage. Here, DDA is held both in PAA cross-linked matrices and on CNF surfaces. The increase

1099114x, 2022, 14, Downloaded from https://onlinelibrary.wiley.com/doi/10.1002/er.7732 by Bartin University, Wiley Online Library on [14/04/2023]. See the Terms and Conditions (https://onlinelibrary.wiley.com/terms-and-conditions) on Wiley Online Library for rules of use; OA articles are governed by the applicable Creative Commons License

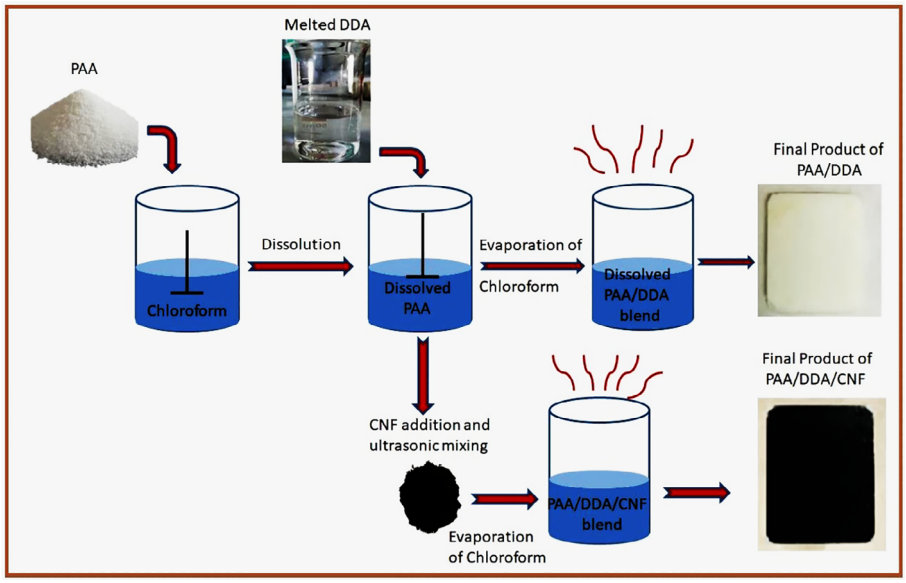

FIGURE 1 The preparation steps for PAA/DDA and PAA/DDA/CNF composites

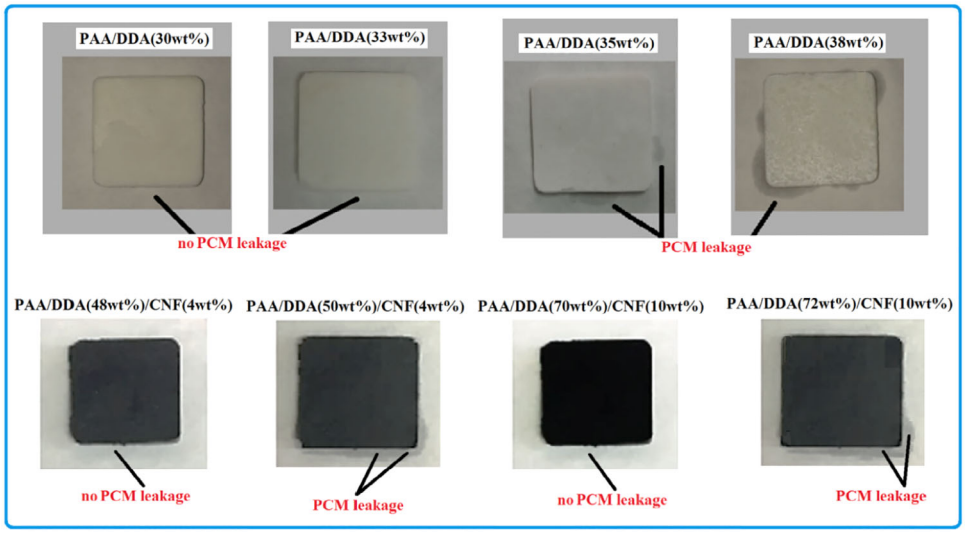

FIGURE 2 The photographs of the produced composite PCMs with/and without CNF additive after shape stabilization test

in the amount of shape-stabilized DDA ratio with boosting the doping amount of CNF may be probably due to the following reasons: (i) the surface area of the cross-linked PAA polymeric network may be increased with homogeneously dispersed CNF and lead to boosting in the confinement rate of DDA; (2) the nanostructured network of CNF may provide an additional scaffold for encapsulation of DDA molecules and (3) the CNF may provide a contribution to the surface tension and capillary forces, which play role in shape-stabilization of DDA.

2.3 | Characterization

The microstructure and morphology of the pure samples and composites were investigated using SEM (Zeiss LEO 440 model). The chemical structures of the composites were investigated by Fourier transform infrared spectroscopy (FTIR, JASCO 430 model). The crystallization behaviour of the composites was identified by X-ray diffraction (XRD) (PANalytical X'-Pert3 model) in the scanning range of 5 to 70°. Melting/freezing points together with the melting/freezing enthalpies for the composite PCMs were obtained by DSC (Hitachi 7020 model) measurements at heating/cooling rates of 3 min/°C under nitrogen atmosphere at a flow rate of 30 mL/min. Thermal stability of the pure DDA, PAA and the shape-stabilized composites were examined carrying out thermal gravimetric analysis (TGA) (PerkinElmer model) analysis at heating speeds of 20°C/min under an argon stream. The thermal reliability of the composites was investigated through a 1000-times repeated thermal cycling operation. The thermal conductivity of samples

1099114x, 2022, 14, Downloaded from https://onlinelibrary.wiley.com/doi/10.1002/er.7732 by Bartin University, Wiley Online Library on [14/04/2023]. See the Terms and Conditions (https://onlinelibrary.wiley.com/terms-and-conditions) on Wiley Online Library for rules of use; OA articles are governed by the applicable Creative Commons License

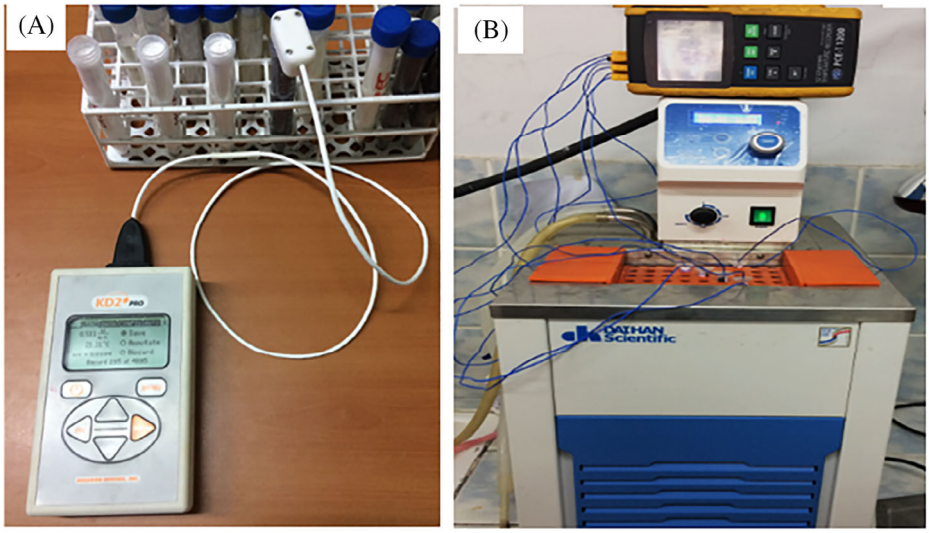

FIGURE 3 Experimental set-up designed for measurement A, thermal conductivity and B, temperature-time data

was gauged by a KD2-Pro Decagon working the principle of heat pulse methodology (Figure 3). The impacts of enhanced thermal conductivity on heat storage and releasing performance were proved through the temperature-time curves obtained using the experimental set-up shown in Figure 3. The samples were introduced into the test tubes and placed in a temperature-controlled water bath. The samples were heated until 35°C to 40°C, and then cooled to 3°C to 5°C. The temperature changes into the sample depending on during both heating and cooling periods were monitored using a thermocouple-data logger system.

3 | RESULTS AND DISCUSSIONS

3.1 | SEM results

SEM images of pure PAA, DDA, CNF, and shape-stabilized composites are presented in Figure 4A-E. As can be seen from the Figure 4A, DDA crystals have a more compact surface, while the PAA surface consists of more irregularly shaped particles with different sizes (Figure 4B). CNF morphology consists of large filamentous heap clusters (Figure 4C. In the morphology of the PAA/DDA composite (Figure 4D), it can be said that compact DDA crystal particles are well wrapped by the amorphous/crystalline PAA cross-linked lattice structure. The CNF dispersion in the PAA/DDA composite was displayed in Figure 4E. As seen from this image, the CNF additive was dispersed homogeneously across the entire surface of the PAA/DDA composite. That the PAA/DDA matrix was wrapped by CNF nanofillers allowed a higher amount of DDA in the composite, that is, here both PAA and CNF helped the shape stabilization of the DDA. The shape stabilizing DDA can be also due to the contributions of both polymeric framework and CNF nano sized-network to the surface tension and capillary forces between DDA molecules and hybrid carrier matrix.

3.2 | FTIR results

FTIR analyses were carried out to examine the chemical structure of the obtained PAA-based composites. The FTIR spectra of the prepared PAA-based composites and their pure components were given in Figure 5. In the FTIR spectrum of the pure DDA, characteristic peaks are seen at wavelengths of 719, 1060, 1467, 2848, 2917 and 3265 cm^{-1}. The absorption peak at 3265 cm^{-1} is caused by O-H stretching vibrations. The spectra at 2917, 2848, and 1467 cm^{-1} arise from the aliphatic C-H stretching and bending vibrations of the methyl and methylene groups. The peak at 1060 cm^{-1} is due to C-O stretching vibration. The characteristic peak at 719 cm^{-1} represents the C-H out-of-plane bending peak.

In the FTIR spectrum of PAA, the characteristic peaks observed at 2936 and 1698 cm^{-1} are due to the non-symmetrical C-H stretching and bending vibrations, respectively. Peaks observed at 1167 and 1413 cm^{-1} correspond to C-O and C=O stretching vibrations, respectively. In addition, the shallower peak observed in the range of 3200 to 3700 cm^{-1} represents the asymmetric stretching vibrations of the O-H group.

In the FTIR spectrum of CNF, characteristic peaks are seen at the wavelengths of 3301, 2842, 1684, 1316 and 1031 cm^{-1}. The characteristic peak at 3301 cm^{-1} is caused by O-H stretching vibration while the peak at 2842 cm^{-1} is due to C-H stretching vibration. The peak detected at 1684 cm^{-1} represents the stretching vibration

1099114x, 2022, 14, Downloaded from https://onlinelibrary.wiley.com/doi/10.1002/er.7732 by Bartin University, Wiley Online Library on [14/04/2023]. See the Terms and Conditions (https://onlinelibrary.wiley.com/terms-and-conditions) on Wiley Online Library for rules of use; OA articles are governed by the applicable Creative Commons License

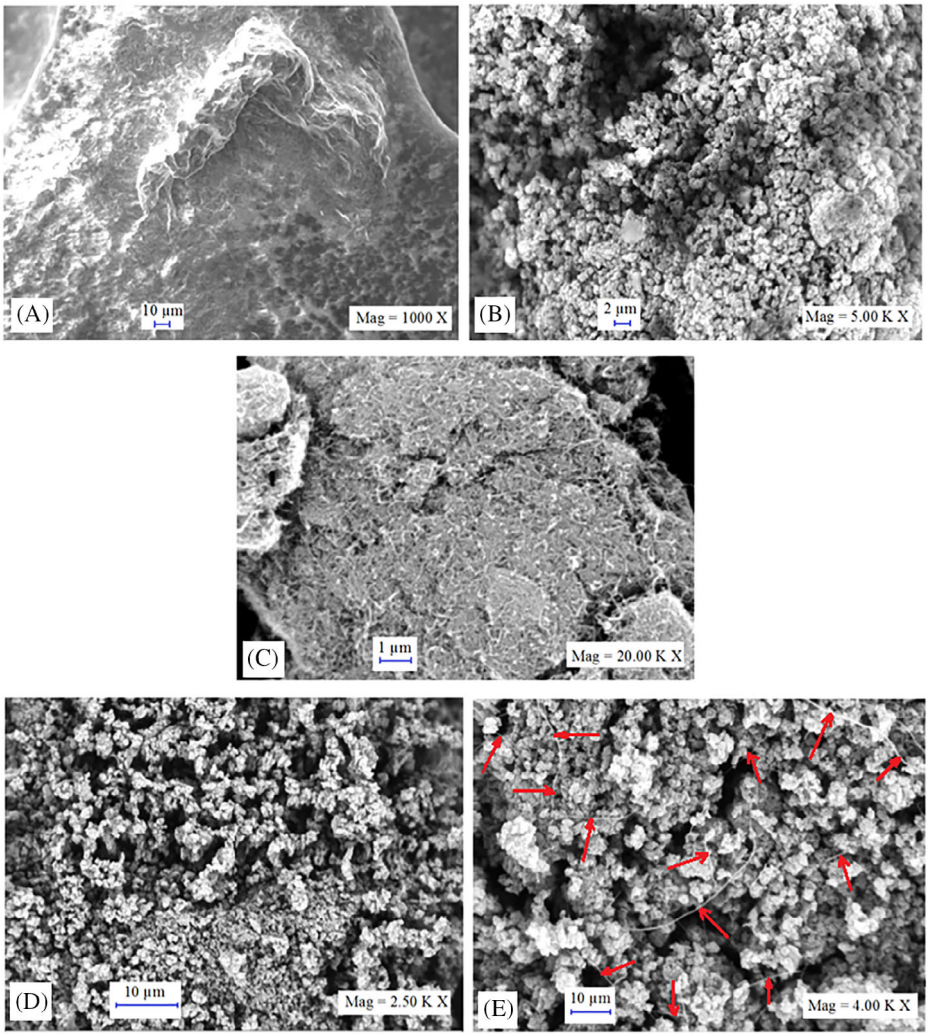

FIGURE 4 SEM photographs of samples A, DDA, B, PAA, C, CNF, D, PAA/DDA(33 wt%) and E, PAA/DDA (70 wt%)/CNF (10 wt%)

band of C=C. The characteristic peaks are seen at 1316 and 1031 cm^{-1} correspond to C-H bending and C-O stretching vibration, respectively.

When inspecting the FTIR spectra of PAA/DDA and PAA/DDA/CNF composites, a peak, which is different from the characteristic peaks of the pure components, was not encountered, and all the existing peaks regarding pure components were detected. However, small shifts in the wavelengths of some characteristic bands of the composites can be noticed. For example; the asymmetric stretching vibration of O-H detected at 3265 cm^{-1} belonging to DDA shifted to 3248 and 3240 cm^{-1} value in spectra of PAA/DDA and PAA/DD/CNF composites, respectively. These small shifts in the wavelength values of the characteristic absorption bands may have been caused by the weak physical intermolecular interactions between component molecules, as well as the interactions between O-H groups in DDA molecules and C-O and C=O groups of PAA molecules. Another possible reason is the hydrogen bridge bond formation that may have formed between the O-H groups belonging to DDA and PAA molecules. All these results prove that there was no chemical interaction between the components of PAA, DDA and CNF.

3.3 | XRD results

XRD diagrams of the produced composite products and pure ingredients are depicted in Figure 6. In the XRD diagram of PAA, the wide peak seen at $2\theta = 12$ to 24° range corresponds to the amorphous phase, but no other peak representing the crystal structure was observed. In the XRD pattern of pure DDA, characteristic peaks belonging to crystal phases were observed at 2θ values of 7.85° (small), 21.55° and 24.50°. In the XRD diagram of CNF, a prominent large peak at 26.01° and a small peak at 35.38° represent CNF crystal structures.

On the other hand, the peaks regarding the crystal structures of the DDA component were recorded at 7.83°, 21.57° and 24.51° in the PAA/DDA composite, while they were detected at 7.85°, 21.54° and 24.53° in the

1099114x, 2022, 14, Downloaded from https://onlinelibrary.wiley.com/doi/10.1002/er.7732 by Bartin University, Wiley Online Library on [14/04/2023]. See the Terms and Conditions (https://onlinelibrary.wiley.com/terms-and-conditions) on Wiley Online Library for rules of use; OA articles are governed by the applicable Creative Commons License

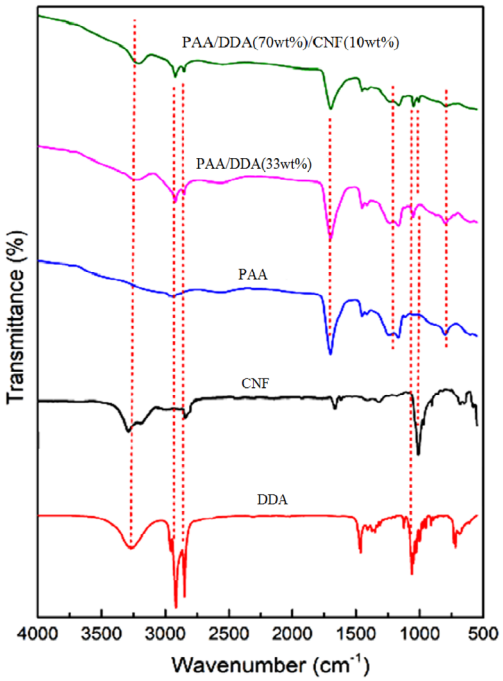

FIGURE 5 FTIR spectrums obtained for PAA/DDA (33 wt%) and PAA/DDA(70 wt%)/CNF (10 wt%) composites, and their components

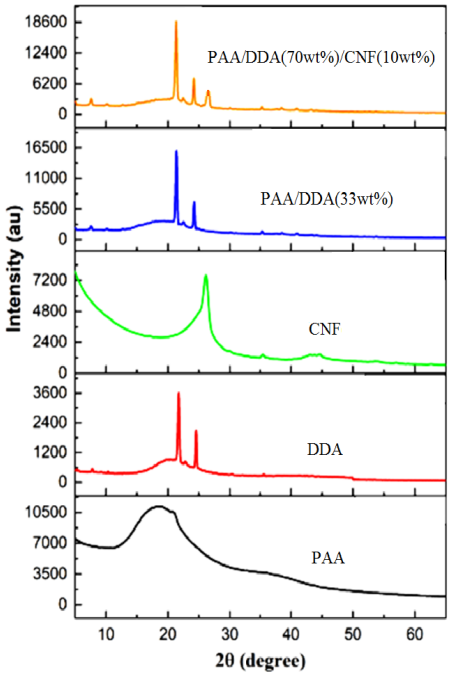

FIGURE 6 XRD diffractograms obtained for PAA/DDA (33 wt %), PAA/DDA (70 wt%)/CNF (10 wt%) composites and their components

PAA/DDA/CNF composite. The small peak seen at 35.33° in the PAA/DDA/CNF composite originated from the crystalline phase of the CNF component. As can be seen from these findings, all of the characteristic peaks representing the crystal structures of the components are also included in the XRD patterns of the composites. This result demonstrated that there was no change in the crystal structures of the components during the preparation of PAA-based composites.

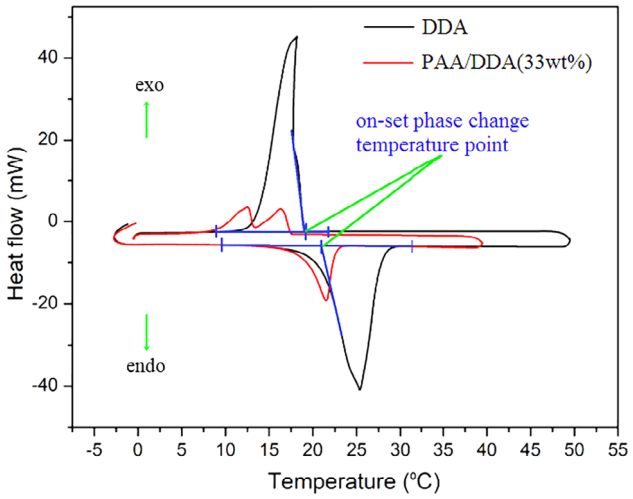

FIGURE 7 Heating and cooling DSC curves of pure DDA and PAA/DDA(33 wt%) composite

3.4 | DSC results

The melting/solidification phase change temperature and latent heat capacities of DDA, PAA/DDA and PAA/DDA/CNF composites were determined on the DSC curves given in Figures 7 and 8. To determine the melting/solidification phase change temperature points, a tangent was drawn from the initial point of the peak such that the maximum slope would be obtained and the point where this tangent intersected the baseline was marked and taken as on-set melting and solidification temperatures. Melting/solidification latent heat capacities were determined by the integration of the areas below the respective peaks. This process was done through DSC software. In this context, measured melting/solidification phase change temperature and enthalpy values for the relevant products were given in Table 1. It can be seen from the DSC curves that PAA/DDA and PAA/DDA/CNF composites exhibit regular melting and solidification behaviour like pure DDA. However, it was observed that these composites showed bimodal exothermic peaks differently from the pure DDA. The bimodal solidification behaviour may probably be due to the solidification of α and β forms of DDA, which is commonly noted during heterogeneous and homogeneous nucleation processes, respectively.[34] Similar bimodal solidification

1099114x, 2022, 14, Downloaded from https://onlinelibrary.wiley.com/doi/10.1002/er.7732 by Bartin University, Wiley Online Library on [14/04/2023]. See the Terms and Conditions (https://onlinelibrary.wiley.com/terms-and-conditions) on Wiley Online Library for rules of use; OA articles are governed by the applicable Creative Commons License

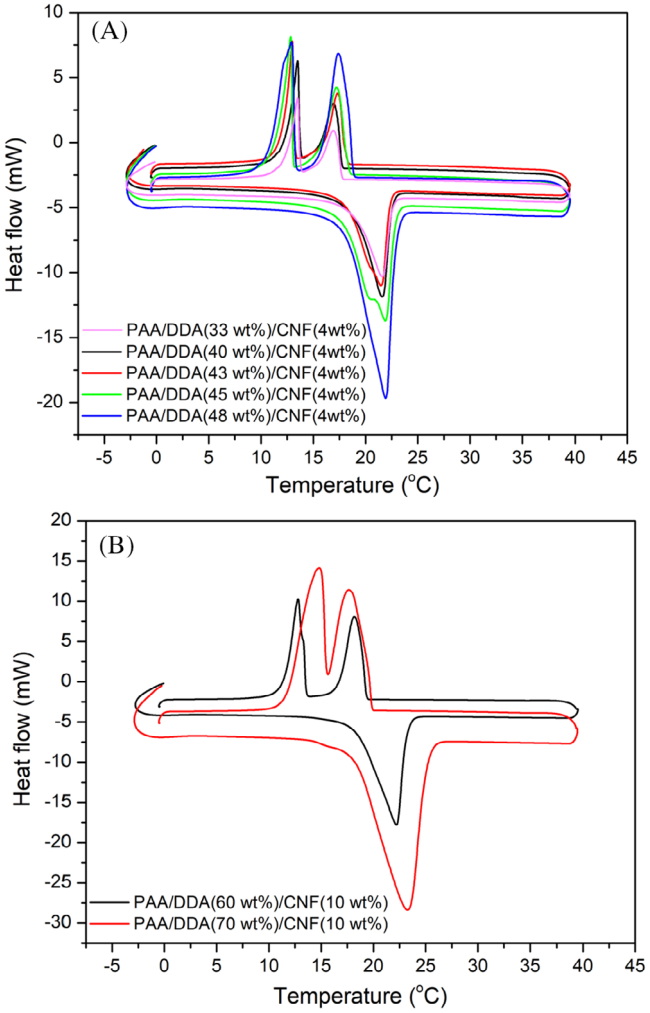

FIGURE 8 Heating and cooling DSC curves of A, PAA/DDA/CNF(4 wt%) composites and B, PAA/DDA/CNF (10 wt%) composites

behaviour was also observed with the microencapsulated PCM samples.[35]

Additionally, according to the data given in Table 1, it is observed that there is a small change in the melting/solidification phase change temperatures of the PAA-based composites compared to pure DDA. The solidification temperature of PAA/DDA(60 wt%)/CNF(10 wt%) and PAA/DDA(70 wt%)/CNF(10 wt%) compared to that of the other composites and pure DDA were slightly higher. These results may be due to the concentrated CNF into the PAA structure may lead to more restrict the crystallization of the DDA molecules.

On the other hand, to investigate the effect of the added CNF, the phase change enthalpy values of the prepared PAA/DDA(33 wt%) and PAA/DDA(33 wt%)/CNF (4 wt%) were also compared in this table. As seen from the depicted values, the melting and solidification latent heats of PAA/DDA(33 wt%) composite were reduced from 75.92 and 77.42 J/g to 74.18 and 75.12 J/g in case of PAA/DDA(33 wt%)/CNF(4 wt%) while the phase change temperature of this composite was slightly altered after doping 4% CNF. Moreover, the measured heat storage capacities of all composites are very compatible with the theoretically calculated values.

Additionally, Table 2 presents a comparison of the LHTES properties of the different polymer-based shape stable composite PCMs reported in the literature with that of PAA/DDA/CNF composite. As can be clearly noticed from tabulated data, the developed PAA/DDA (70 wt%)/CNF(10 wt%) composite has higher than those of all polymer-based composite PCMs given here. This result makes it a promising composite PCM for TES implementations like heat management of buildings, solar thermal power plants, textiles, electronic devices and so on.

3.5 | Thermal reliabilities and structural stabilities of the PAA/DDA and PAA/DDA/CNF composites

The ability of the produced composites to remain thermally and chemically stable after being subjected to the thermal cycle test plays an important role in the use of those composites in real LHTES applications. For this reason, the chemical and thermal stability of the PAA/DDA/CNF(10 wt%) composite, which was selected as the representative of the other composites, was examined by FTIR and DSC analysis after 1000 repetitive melting-solidification processes. As a result of this process, the results of the sample that were not cycle tested and the sample that were cycle tested were compared and checked for any changes.

In this context, comparative FTIR spectra of the PAA/DDA/CNF composite regarding the cycles were given in Figure 9. As can be observed from both spectra, it can be stated that there is no change in the wavelengths and peak appearance of the characteristic peaks. These results revealed that PAA/DDA/CNF composite did not change its chemical structure after 1000 times phase transformation; therefore it has excellent chemical stability.

On the other hand, the effect of the repeated thermal cycling process on the LHTES properties of the PAA/DDA/CNF composite was examined by giving together with the DSC curves of the samples before and after the test in Figure 10. The melting and solidification temperature of PAA/DDA/CNF product after 1000 cycles decreased by 0.05°C and 0.03°C, respectively, while latent

1099114x, 2022, 14, Downloaded from https://onlinelibrary.wiley.com/doi/10.1002/er.7732 by Bartin University, Wiley Online Library on [14/04/2023]. See the Terms and Conditions (https://onlinelibrary.wiley.com/terms-and-conditions) on Wiley Online Library for rules of use; OA articles are governed by the applicable Creative Commons License

TABLE 1 LHTES properties of pure DDA and the produced composite PCMs with/and without CNF additive

Material	Melting temperature (°C)	Latent heat of melting (J/g)	Solidification temperature (°C)	Latent heat of solidification (J/g)
DDA	21.17	234.01	19.22	234.03
PAA/DDA(33 wt%)	18.09	75.92	17.50	77.42
PAA/DDA(33 wt%)/CNF(4 wt%)	18.30	74.18	17.80	75.12
PAA/DDA(40 wt%)/CNF(4 wt%)	18.34	92.71	17.82	92.31
PAA/DDA(43 wt%)/CNF(4 wt%)	18.14	97.83	18.08	99.50
PAA/DDA(45 wt%)/CNF(4 wt%)	18.12	101.91	18.42	103.11
PAA/DDA(48 wt%)/CNF(4 wt%)	18.11	112.02	18.93	113.02
PAA/DDA(60 wt%)/CNF(10 wt%)	18.18	136.01	19.42	135.03
PAA/DDA(70 wt%)/CNF(10 wt%)	18.04	157.03	19.86	158.01

TABLE 2 Comparing the LHTES properties of the PAA/DDA/CNF composite with literature

Composite PCM	Melting temperature (°C)	Solidification temperature (°C)	Latent heat of fusion (J/g)	Reference
Polyester resin/PEG/GNP	52.8	36.7	140.80	2
Polypyrrole/palmitic acid/ GNP	61.0	61.3	151	20
Polyvinyl butyral/palmitic acid/expanded graphite	56.1	59.4	122.05	22
PMMA/fatty acid eutectic	21.11 to 34.81	-	59.29 to 80.75	23
PMMA/paraffin	21.8	-	142.7	35
Polyaniline/myristic acid	57.35	-	150.63	36
PMMA/stearic acid	60.4	50.6	92.1	37
Polypropylene/paraffin	44.77	53.55	136.16	38
PAA/DDA(70 wt%)/CNF(10 wt%)	18.04	19.86	157.03	This study

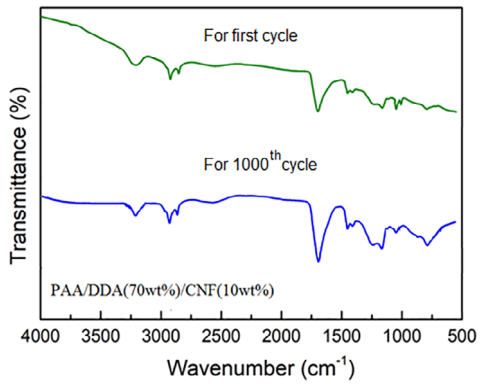

FIGURE 9 FTIR spectrum of PAA/DDA (70 wt%)/CNF (10 wt %) composite obtained for 0th and 1000th cycle

heat capacities only decreased by about 2.1% compared to the non-cycled sample. Based on these values, it can be concluded that the PAA/DDA/CNF composite has a very good thermal reliability after 1000 times the thermal cycling process.

3.6 | TGA results

TGA curves of pure DDA, PAA and prepared composites of PAA/DDA (33 wt%) and PAA/DDA (70 wt%)/CNF (10 wt%) were demonstrated in Figure 11. It is observed that pure DDA undergoes thermal decomposition (with about 100% mass loss) in a single step in the range of 160°C to 255°C. PAA is decomposed into two steps: the first step occurs between 200°C and 340°C while the second step corresponds to the temperature range of 340°C to 520°C. The CNF shows little weight loss (about 5%) up to 130°C probably due to humidity retained within the nanofiber network. Also, it does not indicate any thermal degradation up to 600°C. On the other hand, PAA/DDA (33 wt%) composite decomposed at three-stage in the range of about 125°C to 520°C, the first one at 125°C to 200°C includes the first weight loss (32.8%,) which is belonging to the DDA. The second one at 200°C to 340°C is associated with the first step degradation (22.8%) of PAA. The third decomposition step of this composite is carried out between 340°C and 520°C. Moreover, in the

1099114x, 2022, 14, Downloaded from https://onlinelibrary.wiley.com/doi/10.1002/er.7732 by Bartin University, Wiley Online Library on [14/04/2023]. See the Terms and Conditions (https://onlinelibrary.wiley.com/terms-and-conditions) on Wiley Online Library for rules of use; OA articles are governed by the applicable Creative Commons License

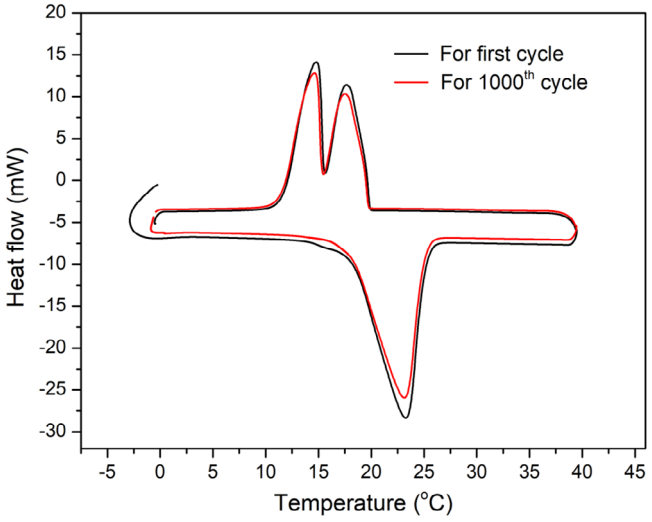

FIGURE 10 Heating and cooling DSC curves of PAA/DDA (70 wt%)/CNF (10 wt%) composite obtained for 0th and 1000th cycle

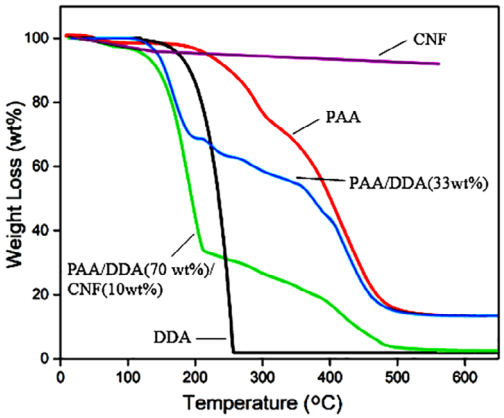

FIGURE 11 TGA curves of DDA, PAA, CNF, PAA/DDA (33 wt%) and PAA/DDA(70 wt%)/CNF (10 wt%) composites

case of PAA/DDA(70 wt%)/CNF(10 wt%) composite, the first, second and third degradation steps are taken place in the range of 125°C to 210°C, 210°C to 390°C and 390°C to 540°C, respectively. The first step corresponds to 68.2% and the total weight losses regarding the other steps are about 31%. The PAA component of the composite significantly did not influence the thermal decomposition temperature of DDA while the CNF additive slightly affected the initial and ending decomposition temperatures of DDA and PAA. Furthermore, the first-step decomposition temperatures of both composite PCMs are still much more above the operating temperature or phase change temperature of DDA (about 18°C-20°C).

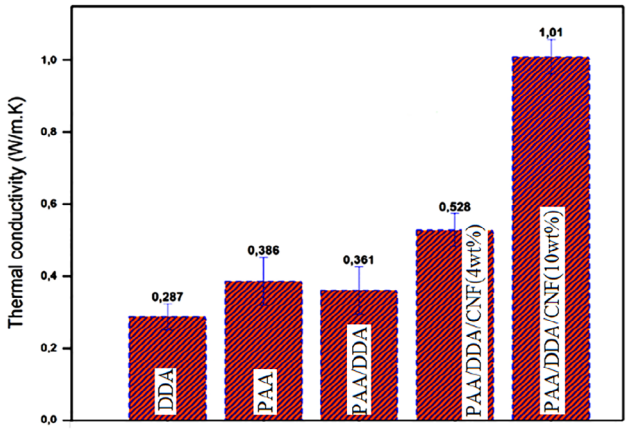

FIGURE 12 Thermal conductivity results of DDA, PAA, PAA/DDA(33 wt%), PAA/DDA(48 wt%)/CNF (4 wt%) and PAA/DDA(70 wt%)/CNF (10 wt%)

3.7 | Thermal conductivity results

One of the features that limit the use of organic PCMs in various applications is their thermal conductivity. Increasing the thermal conductivity of PCMs, that is, increasing the heat storage/release speeds, paves the way for their use in different applications. In this context, the measured thermal conductivity of the pure PAA, DDA and the prepared composites were given in Figure 12. As can be noticed, doping of the prepared PAA/DDA composite with 4 and 10 wt% CNF caused significant increases in thermal conductivity. According to the results, an increase of 46.26% was obtained with the addition of 4 wt% CNF to the PAA/DDA composite compared with the measured thermal conductivity value for PAA/DDA. For the same sample, the addition of 10 wt% CNF provided an increase of 179.77%. These increases can be attributed to the fact that CNF, which has significantly high thermal conductivity, disperses homogeneously in the composite and creates heat transfer paths at different points along the composite surface. Besides, the comparison of the thermal conductivity of PAA-based composites with the various polymer-based composite PCMs reported in the literature was given Table 3.

As can be seen from the table, different types of additives have been used in the literature to improve the thermal conductivity of different polymer/PCM composites. It can be inferred that the thermal conductivity values of 4 and 10 wt% CNF added PAA/DDA composites produced in this study are high enough to be comparable to the values reported for different types of polymer/PCM/carbon-based additive composites.

Additionally, temperature-time curves of pure DDA, PAA/DDA(33 wt%), PAA/DDA(48 wt%)/CNF(4 wt%) and PAA/DDA(70 wt%)/CNF(10 wt%) composites were

1099114x, 2022, 14, Downloaded from https://onlinelibrary.wiley.com/doi/10.1002/er.7732 by Bartin University, Wiley Online Library on [14/04/2023]. See the Terms and Conditions (https://onlinelibrary.wiley.com/terms-and-conditions) on Wiley Online Library for rules of use; OA articles are governed by the applicable Creative Commons License

TABLE 3 Comparing the thermal conductivity of the PAA-based composites with literature

Polymer	PCM	Additive (wt%)	Thermal conductivity (W/mK)	Reference
Polyester resin	PEG	GNP (2)	0.67	2
Polypyrrole	Palmitic acid	GNP (1.6)	0.43	20
HDPE	Palmitic acid	GNP (4)	0.82	21
Polyvinyl butyral	Palmitic acid	Expanded graphite (7)	0.51	22
Polyaniline	Palmitic acid	Graphite nanoplatelets (7.87)	1.08	30
HDPE	Stearyl alcohol	Expanded graphite (3)	0.66	39
HDPE	Myristic acid	Nano-Al_2O_3 (12)	0.39	40
HDPE	Myristic acid	Nano-graphite (12)	0.45	40
PAA	DDA	-	0.36	This study
PAA	DDA	CNF (4)	0.52	This study
PAA	DDA	CNF (10)	1.01	This study

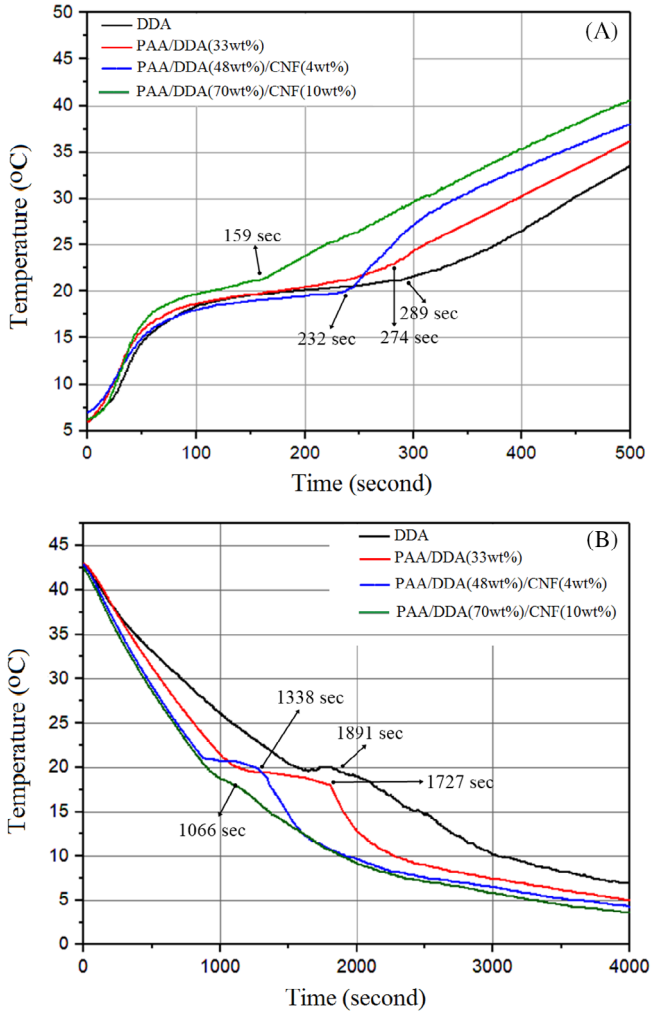

FIGURE 13 Heating and cooling time–temperature curves obtained for DDA, PAA/DDA(33 wt%), PAA/DDA(48 wt%)/CNF (4 wt%) and PAA/DDA(70 wt%)/CNF (10 wt%)

presented in Figure 13 to prove the obtained thermal conductivity increments. In the specification of the heat storage and release speed of the samples, the times corresponding to the points at which the curves show breaking with the completion of the phase changes were taken as a basis. In the heating period, the time taken to reach the defined breakpoints was found to be as 289, 274, 232 and 159 s, respectively, for pure DDA, PAA/DDA(33 wt%), PAA/DDA(48 wt%)/CNF(4 wt%) and PAA/DDA(70 wt%)/CNF(10 wt%) samples. In the cooling period, these times were found to be as 1891, 1727, 1338 and 1066 s, respectively, for pure DDA, PAA/DDA(33 wt%), PAA/DDA(48 wt%)/CNF(4 wt%) and PAA/DDA(70 wt%)/CNF(10 wt%) samples. These results mean that the heat storage and release performance of the PAA/DDA composite was improved by 15.32% and 22.52%, respectively, with 4%wt CNF. A 10 wt % CNF doping enhanced the heat storage and release performance of the PAA/DDA composite by 41.97% and 38.27%, respectively. These data indicate that the effect of CNF nanofiller on the enrichment of thermal conductivity of PAA/DDA composite was also verified by the heat storage and release performance test.

4 | CONCLUSIONS

In this paper, shape-stabilized PAA/DDA and PAA/DDA/CNF composite PCMs with melting temperatures in the range of 18.04°C to 18.34°C and latent heat capacities in the range of 75.92 to 157.03 J/g were prepared by solution blending technique. Herein, PAA was introduced as a sole supporter material for the first time

1099114x, 2022, 14, Downloaded from https://onlinelibrary.wiley.com/doi/10.1002/er.7732 by Bartin University, Wiley Online Library on [14/04/2023]. See the Terms and Conditions (https://onlinelibrary.wiley.com/terms-and-conditions) on Wiley Online Library for rules of use; OA articles are governed by the applicable Creative Commons License

in the production of thermally conductive novel composite PCMs doped with CNF. The mass rate of DDA in the PAA/DDA/CNF(10 wt%) composite is as high as 70 wt% without a leak. This was not only achieved with PAA, but CNF helped reduce DDA leakage in the composite PCMs by wrapping PAA/DDA blends. The FTIR and XRD results revealed that the PAA-based composite PCMs have a consistent chemical structure and well-remained crystallization behaviours. Microstructure analysis indicated that DDA was well-wrapped by PAA, and CNF was uniformly dispersed in the composite. A-600 thermal cycle test was not gave any damage to the chemical structure or LHTES characteristics of the composite PCM. TGA results exhibit satisfactory thermal reliability properties, which were stable up to 115°C. The shape-stabilized PAA/DDA composites doped with CNF possess improved thermal conductivity, that is, fast heat storing and releasing performance. The thermal conductivity of the PAA/DDA composite doped with 4 and 10 wt% CNF was increased by 46.26% and 179.77% compared to pure PAA/DDA composite. In summary, satisfying shape stabilization performance, the improved thermal conductivity, superior thermal characteristics, well-remained chemical structure stand out the novel PAA-based composite PCMs as promising materials in the field of many TES applications.

ORCID

Ahmet Sarı https://orcid.org/0000-0002-7452-083X

REFERENCES

1. Song M, Niu F, Mao N, Hu Y, Deng S. Review on building energy performance improvement using phase change materials. *Energ Buildings*. 2018;158:776-793.
2. Zhao Y, Min X, Huang Z, Liu Y, Wu X, Fang M. Honeycomb-like structured biological porous carbon encapsulatingPEG: a shape-stable phase change material with enhanced thermalconductivity for thermal energy storage. *Energ Buildings*. 2018;158:1049-1062. doi:10.1016/j.enbuild.2017.10.078
3. Ali Memon S, Yiu Lo T, Shi X, Barbhuiya S, Cui H. Preparation, characterization and thermal properties of lauryl alcohol/kaolin as novel form-stable composite phase change material for thermal energy storage in buildings. *Appl Therm Eng*. 2013;59:336-347. doi:10.1016/j.applthermaleng.2013.05.015
4. Ghadim HB, Shahbaz K, Al-Shannaq R, Farid MM. Binary mixtures of fatty alcohols and fatty acid esters as novel solid-liquid phase change materials. *Int J Energy Res*. 2019;43:8536-8547.
5. Konuklu Y, Ersoy O, Erzin F. Development of pentadecane/diatomite and pentadecane/sepiolite nanocomposites fabricated by different compounding methods for thermal energy storage. *Int J Energy Res*. 2019;43:6510-6520.
6. Qian T, Li J, Min X, Deng Y, Guan W, Ma H. Polyethylene glycol/mesoporous calcium silicate shape-stabilized composite phase change material: preparation, characterization, and adjustable thermal property. *Energy*. 2015;82:333-340.
7. Seki Y, Ince S, Ezan MA, Turgut A, Erek A. Development and evaluation of graphite nanoplate (GNP)-based phase change material for energy storage, applications. *Int J Energy Res*. 2015;39:696-708.
8. Gao J, Zhou J, Zhang X, Shi Q, Han Z, Chen Y. Facile functionalized mesoporous silica using biomimetic method as new matrix for preparation of shape-stabilized phase-change material with improved enthalpy. *Int J Energy Res*. 2019;43:8649-8659.
9. Khadiran T, Hussein MZ, Zainal Z, Rusli R. Encapsulation techniques for organic phase change materials as thermal energy storage medium: a review. *Sol Energy Mater Sol Cells*. 2015;143:78-98. doi:10.1016/j.solmat.2015.06.039
10. Kenisarin MM, Kenisarina KM. Form-stable phase change materials for thermal energy storage. *Renew Sust Energ Rev*. 2012;16:1999-2040. doi:10.1016/j.rser.2012.01.015
11. Cheng F, Zhang X, Wen R, et al. Thermal conductivity enhancement of form-stable tetradecanol/expanded perlite composite phase change materials by adding cu powder and carbon fiber for thermal energy storage. *App Therm Eng*. 2019;156:653-659. doi:10.1016/j.applthermaleng.2019.03.140
12. Jia W, Wang C, Wang T, Cai Z, Chen K. Preparation and performances of palmitic acid/diatomite form-stable composite phase change materials. *Int J Energy Res*. 2020;44(6):4298-4308.
13. Hekimoğlu G, Nas M, Ouikhalfan M, et al. Thermal management performance and mechanical properties of a novel cementitious composite containing fly ash/lauric acid-myristic acid as form-stable phase change material. *Constr Build Mater*. 2021;274:122105. doi:10.1016/j.conbuildmat.2020.122105
14. Sarı A, Ouikhalfan M, Chehouani H, et al. Form-stabilized polyethylene glycol/Palygorskite composite phase change material: thermal energy storage properties, cycling stability, and thermal durability. *Polym Eng Sci*. 2020;60(5):909-916.
15. Sarı A, Biçer A, Hekimoğlu G. Effects of carbon nanotubes additive on thermal conductivity and thermal energy storage properties of a novel composite phase change material. *J Compos Mater*. 2019;53(21):2967-2980.
16. Zhao Y, Sun B, Du P, et al. Hierarchically channel-guided porous wood-derived shape stabilized thermal regulated materials with enhanced thermal conductivity for thermal energy storage. *Mater Res Express*. 2019;6:115515. doi:10.1088/2053-1591/ab4700
17. Min X, Fang M, Huang Z, et al. Enhanced thermal properties of novel shape-stabilized PEG composite phase change materials with radial mesoporous silica sphere for thermal energy storage. *Sci Rep*. 2015;5:12964. doi:10.1038/srep12964
18. Sarı A, Alkan C, Biçer A, Bilgin C. Latent heat energy storage characteristics of building composites of bentonite clay and pumice sand with different organic PCMs. *Int J Energy Res*. 2014;38:1478-1491.
19. Tang B, Wang L, Xu Y, Xiu J, Zhang S. Hexadecanol/phase change polyurethane composite as form-stable phase change material for thermal energy storage. *Sol Energy Mater Sol Cells*. 2016;144:1-6.
20. Silakhori M, Fauzi H, Mahmoudian MR, Metselaar HSC, Mahlia TMI, Khanlou HM. Preparation and thermal properties of form-stable phase change materials composed of palmitic acid/polypyrrole/graphene nanoplatelets. *Energ Buildings*. 2015;99:189-195.
21. Tang Y, Jia Y, Alva G, Huang X, Fang G. Synthesis, characterization and properties of palmitic acid/high density

1099114x, 2022, 14, Downloaded from https://onlinelibrary.wiley.com/doi/10.1002/er.7732 by Bartin University, Wiley Online Library on [14/04/2023]. See the Terms and Conditions (https://onlinelibrary.wiley.com/terms-and-conditions) on Wiley Online Library for rules of use; OA articles are governed by the applicable Creative Commons License

polyethylene/graphene nanoplatelets composites as form-stable phase change materials. *Sol Energy Mater Sol Cells*. 2016;155:421-429.
22. Lin Y, Zhu C, Alva G, Fang G. Palmitic acid/polyvinyl butyral/expanded graphite composites as form-stable phase change materials for solar thermal energy storage. *Appl Energy*. 2018;228:1801-1809.
23. Wang L, Meng D. Fatty acid eutectic/polymethyl methacrylate composite as form-stable phase change material for thermal energy storage. *Appl Energy*. 2010;87:2660-2665.
24. Resch-Fauster K, Feuchter M. Thermo-physical characteristics, mechanical performance and long-term stability of high temperature latent heat storages based on paraffin-polymer compounds. *Thermochim Acta*. 2018;663:34-45. doi:10.1016/j.tca.2018.03.004
25. Chen F, Wolcott M. Polyethylene/paraffin binary composites for phase change material energy storage in building: a morphology, thermal properties, and paraffin leakage study. *Sol Energy Mater Sol Cells*. 2015;137:79-85.
26. Kee S, Munusamy Y, Ong K, Cornelis Metselaar H, Chee S, Lai K. Thermal performance study of composite phase change material with Polyacrylicand conformal coating. *Materials*. 2017;10:873. doi:10.3390/ma10080873
27. Chen C, Wang L, Huang Y. Role of M n of PEG in the morphology and properties of electrospun PEG/CA composite fibers for thermal energy storage. *AICHE J*. 2009;55:820-827. doi:10.1002/aic.11708
28. Jose J, Shehzad F, Al-Harthi MA. Preparation method and physical, mechanical, thermal characterization of poly(vinyl alcohol)/poly(acrylic acid) blends. *Polym Bull*. 2014;71:2787-2802. doi:10.1007/s00289-014-1221-3
29. Tian B, Yang W, Luo L, et al. Synergistic enhancement of thermal conductivity for expanded graphite and carbon fiber in paraffin/EVA form-stable phase change materials. *Sol Energy*. 2016;127:48-55.
30. Zeng JL, Zheng SH, Yu SB, et al. Preparation and thermal properties of palmitic acid/polyaniline/exfoliated graphite nanoplatelets form-stable phase change materials. *Appl Energy*. 2014;115:603-609.
31. Alkan C, Günther E, Hiebler S, Himpel M. Complexing blends of polyacrylic acid-polyethylene glycol and poly(ethylene-co-acrylic acid)-polyethylene glycol as shape stabilized phase change materials. *Energy Convers Manag*. 2012;64:364-370. doi:10.1016/j.enconman.2012.06.003
32. Wong JLO, Munusamy Y, Yu GQ, Kee SY, Seng OK. Performance of form-stable myristic acid/polymethyl methacrylate composite phase-change material coated with nitrile butadiene rubber/polyacrylic acid layered coatings. *J Appl Polym Sci*. 2020;137(18):48642.
33. Baştürk E, Kahraman MV. Thermal and phase change material properties of comb-like Polyacrylic acid-grafted-fatty alcohols. *Polym-Plast Technol Eng*. 2018;57(4):276-282.
34. Singh J, Parvate S, Dixit P, Chattopadhyay S. Facile synthesis of microencapsulated 1-dodecanol (PCM) for thermal energy storage and thermal buffering ability in embedded pvc film. *Energy Fuel*. 2020;34(7):8919-8930. doi:10.1021/acs.energyfuels.0c01019
35. Geng L, Wang S, Wang T, Luo R. Facile synthesis and thermal properties of nanoencapsulated n-dodecanol with sio2 shell as shape-formed thermal energy storage material. *Energy Fuel*. 2016;30:6153-6160. doi:10.1021/acs.energyfuels.6b00929
36. Meng D, Zhao K, Wang A, Wang B. Preparation and properties of paraffin/PMMA shape-stabilized phase change material for building thermal energy storage, journal Wuhan University of Technology. *Mater Sci Ed*. 2020;35:231-239.
37. Zeng J-L, Zhu F-R, Yu S-B, et al. Myristic acid/polyaniline composites as form stable phase change materials for thermal energy storage. *Sol Energy Mater Sol Cells*. 2013;114:136-140. doi:10.1016/j.solmat.2013.03.006
38. Wang Y, Xia TD, Feng HX, Zhang H. Stearic acid/polymethylmethacrylate composite as form-stable phase change materials for latent heat thermal energy storage. *Renew Energy*. 2011;36(6):1814-1820.
39. Tang Y, Lin Y, Jia Y, Fang G. Improved thermal properties of stearyl alcohol/high density polyethylene/expanded graphite composite phase change materials for building thermal energy storage. *Energ Buildings*. 2017;153:41-49.
40. Tang Y, Su D, Huang X, Alva G, Liu L, Fang G. Synthesis and thermal properties of the MA/HDPE composites with nano-additives as form-stable PCM with improved thermal conductivity. *Appl Energy*. 2016;180:116-129.

How to cite this article: Hekimoğlu G, Sarı A, Gencel O, Tyagi VV. Thermal energy storage characteristics of polyacrylic acid/dodecanol/carbon nanofiber composites as thermal conductive shape-stabilized composite phase change materials. *Int J Energy Res*. 2022;46(14):20873-20885. doi:10.1002/er.7732

1099114x, 2022, 14, Downloaded from https://onlinelibrary.wiley.com/doi/10.1002/er.7732 by Bartin University, Wiley Online Library on [14/04/2023]. See the Terms and Conditions (https://onlinelibrary.wiley.com/terms-and-conditions) on Wiley Online Library for rules of use; OA articles are governed by the applicable Creative Commons License